Turkish Journal of Electrical Engineering & Computer Sciences

http://journals.tubitak.gov.tr/elektrik/

Research Article

Turk J Elec Eng & Comp Sci
(2021) 29: 1582 – 1597

doi:10.3906/elk-2007-46

A new design algorithm for the PMHS motor considering the combination ratio

Ali BEHNIAFAR[1,*], **Ahmad DARABI**[2]

[1]Department of Electrical and Electronics Engineering, Faculty of Engineering, Gonbad Kavous University, Gonbad Kavous, Iran

[2]Department of Electrical and Electronics Engineering, Faculty of Electrical and Robotics Engineering, Shahrood University of Technology, Shahrood, Iran

Received: 07.07.2020 • **Accepted/Published Online:** 09.10.2020 • **Final Version:** 31.05.2021

Abstract: Recently, the hysteresis motors have a special significance in the nuclear industries. This is because these motors have some advantages such as low noise, high mechanical strength and group feeding ability. They also have some disadvantages that make some limitations for related industries. These disadvantages include low synchronization torque, low power factor, low efficiency, and hunting. One solution to reduce these disadvantages is to combine the hysteresis motor with the PM motor. This however requires a correct and flexible design procedure as well as an appropriate choice of the machine structure. Accordingly, this paper aims to present a new design algorithm for a disc-type permanent magnet hysteresis synchronous (PMHS) hybrid motor. The proposed design algorithm not only tries to retain the positive features of the both motors in the resulted hybrid motor, but it also gives the user the option of determining the percentage of the combination of the two motors. In other words, the user can determine the contribution of each motor to the output power of the resulted motor. The proposed algorithm is finally validated through fabricating a prototype disc-type PMHS motor and evaluating its performance by simulation and experiment.

Key words: PMHS motor, hysteresis motor, PM motor, design algorithm

1. Introduction

Hysteresis motors are usually constructed in small and very small powers and for high speed applications [1]. Their rotors are made of high-hysteresis materials. These synchronous motors are self-starting. Some of their significant advantages are high mechanical strength, low-noise level and uniform torque from start-up to synchronization which made them suitable for high-speed applications such as the nuclear industries. Various motors are used in nuclear centrifuges, the most common of which are BLDC motors and hysteresis motors. The main problem with BLDC motors is that they require a rotor position sensor. This problem has severely limited the group feeding of these motors. So for each BLDC motor, a drive is required. On the other hand, the hysteresis motors do not require a rotor position sensor and therefore can be fed in groups. In addition, due to the self-starting feature of hysteresis motors (rotor induction property), the rotor disc can also play a damping role at synchronous speed. Also, low noise, simple and integrated structure and high mechanical strength of rotor of the hysteresis motor rotor are among the reasons that have made the nuclear industry interested. Beside these benefits, some drawbacks such as the very low level of output torque, low efficiency and low power factor have limited the related industries of hysteresis motors. Moreover, unlike other synchronous motors, the hysteresis motor has no specific synchronization point, which causes low frequency oscillations

*Correspondence: ali_behniafar@yahoo.com

around the synchronous speed. This phenomenon is called hunting. To overcome these limitations, several methods have been proposed so far. The most effective of them is the combination of hysteresis motor with the other motors. The PM and reluctance motors are some synchronous motors used for combination with hysteresis motors. The reluctance motors by themselves have low levels of output torque, efficiency and power factor. Hence, combining them with the hysteresis motor does not meet the combination goals properly. For this reason, such structure has not drawn attention of the researchers. On the other hand, a PM motor has a high level of output torque, efficiency and power factor. So its combination with a hysteresis motor can potentially yield a motor with a highly desirable performance. The challenge for this combination is that the power densities of the PM motors are very high and those of the hysteresis motors are very low. Therefore, their combination leads to many dimensional restrictions that will greatly affect the performance of the resulted hybrid motor. In this paper, it has been demonstrated that such limitations can be resolved by choosing the appropriate structure and flexible design. First it is useful to investigate briefly the most significant researches published so far in this field. The PMHS motor was at first fabricated by Perov in 1959 [2]. That motor had a cylindrical rotor, which was designed through installing the permanent magnets on the hysteresis ring. Perov showed that the use of permanent magnets in the rotor of hysteresis motor eliminates many of its shortcomings including low power factor, low efficiency and oscillations around synchronous speed. In 1984, Rahman et al. investigated the effect of adding samarium-cobalt permanent magnets to a cylindrical hysteresis motor [3]. They also showed that the use of this magnet would yield a greater airgap excitation voltage than the other magnets like Alnico 5, and eventually would improve the machine performance. Since the hysteresis rings are usually made as foils, grooving the hysteresis ring and installing magnets on it, involves many difficulties. Nevertheless, the basic problem in the proposed motor structure of this paper is that the path of closing the magnet flux has not been properly selected. In this structure, magnets have been placed in the radial direction, and on the other hand, the magnet holder has been chosen from nonmagnetic materials, which weakens the flux of the magnet. Moreover, in 1985, the steady state performance of the cylindrical hysteresis reluctance motor with a new structure was investigated [4]. The magnetic saliency in this structure has been created through grooving the inner surface of the hysteresis ring. The dominant relations on the reluctance hysteresis motor were also extracted using the d-q axes theory. Then, by comparing the analytical and experimental results, it was shown that the hysteresis reluctance motor has better characteristics in terms of efficiency, power factor and the maximum torque compared to the conventional hysteresis motor. In 1990, the dynamic and steady state behaviors of the reluctance hysteresis motor with the structure introduced in [4] in the single-phase supplying mode with phase-compensating capacitors was investigated [5]. In this study, the process of proper choosing of compensating capacitors is presented to reduce the synchronization time. It was also shown that when the motor is supplied with the single-phase power with proper phase balancing capacitors has an appropriate performance rather than three-phase power supply. In 1991, Rahman built and patented the cylindrical permanent magnet hysteresis motor through adding a permanent magnet to the hysteresis ring [6]. This structure has the same characteristics as the structure of [3]. The PMHS motor with the same structure introduced in [6] was then investigated in 1996 and its behavior was predicted using the state variables of the motor in the time domain [7]. Such a method has been employed because the previous analytical methods (based on the rotor reference frame and modeling of the permanent magnet and hysteresis materials by an electric motive force) cannot easily characterize the machine behavior when the parameters are unbalanced or nonlinear. In 2003 [8], the magnetic equivalent circuits of the d-q axes for the structure introduced in [6] was extracted, based on which, a control strategy was designed for the PMHS motor. The model of the PMHS motor with the structure of [6] was then

analyzed in [9] using the finite element method. In this research, the Potter's and Schmulian's model has been used to approximate the hysteresis loop. In [10], a disc-type PMHS motor was introduced and manufactured. In this reference, the analytical model of PMHS motor was presented and verified by experimental results. Also, in [11] a numerical method was applied for analyses of steady state of the PMHS motor. Some other researches have also been accomplished about the PMHS motor, which are briefly explained here. Rahman and Qin studied the application of the PMHS motor versus the other motors for using in electric vehicles [12]. They also conducted some researches on PMHS motor control [13, 14]. Nassiri et al. [15] and Lesani et al. [16] have published some researches about the control of hunting phenomenon and fast control of PMHS motor respectively. In [17, 18], the equivalent magnetic and electric circuits in the d-q system and also a control strategy were introduced for a cylindrical permanent magnet hysteresis motor. It should be noted that in all the previous researches, there has been no mention of the design of the PMHS motor and its dimensional limitations. Moreover, the magnets used in these researches were made of the high-energy types or the low-energy types with large dimensions. This intensifies the problem of unequal power density and thus makes the performance of the resulted hybrid motor undesirable. It is clear that in a certain output power, the motors with different power densities have different dimensions. Furthermore, the effect of one on the number of winding turns, stator core thickness, etc. impairs the performance of the other. Hence their combination will not yield satisfactory results. In this paper a new design algorithm for the disc-type PMHS hybrid motor is presented. In this algorithm, the contribution ratio of combination is considered as input data of design that can resolve most of the problems of combination. In this regard, in the next section, the disc-type structure of the studied PMHS motor is introduced and the stages of the proposed design algorithm are described. The presented design algorithm has been implemented for various contribution ratios, whose results are given in Section 3. In Section 4, based on the input data of the design algorithm, a prototype disc-type PMHS motor has been designed and fabricated. Also the experimental and analytical results of studied motor are compared to each other. Finally, the conclusion is given in Section 5.

2. Structure selection and design of the disc-type PMHS motor

So far, no design algorithms for the PMHS motor have been presented for any of its structures. Hence, in this section, the design algorithm of the disc-type PMHS motor is presented and then a prototype disc-type PMHS motor is designed. The proposed design algorithm allows the user to set the percentage of the influence of each motor in the resulted hybrid PMHS motor. In other words, the user can specify the contribution ratio of each of the two motors (hysteresis and PM) to the output power of the PMHS motor. Choosing an appropriate structure is very significant because it has a great impact on retaining the essential advantages of the two motors in the resultant hybrid motor. Various structures can be considered for PMHS motors. The structure discussed in this paper is the same structure presented in [10]. It consists of a slotless stator with a thyroidal winding and a rotor having two discs. One disc is made of hysteresis material and the other disc is assembled of the magnets placed on the surface of a ferromagnetic holder. This structure is shown in Figure 1a.

Now, the design algorithm of the PMHS motor is presented considering the following assumptions:

1) The direction of the magnetic field in the airgaps is completely axial and in the hysteresis and magnet holder discs is absolutely circumferential (Figure 1b).

2) The magnetic field in the hysteresis disc and the magnet holder disc has a uniform distribution along axial direction.

3) The hysteresis loops of the rotor disc have been approximated by using a set of concentric ellipses.

4) The design process is performed for steady state conditions with maximum synchronization torque.

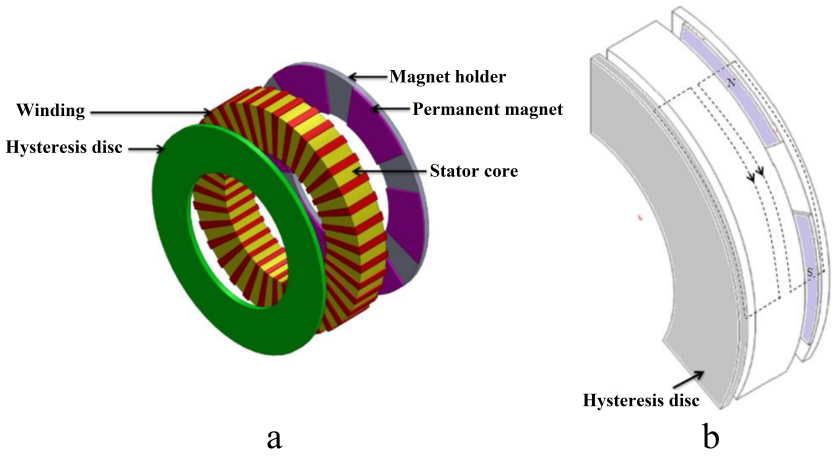

Figure 1. a) Structure of the disc-type PMHS motor [10], b) flux direction in structure of disc-type PMHS motor.

The reason for choosing the fourth assumption is that in partial load conditions the operational hysteresis loops do not match the main loops of the rotor material. This is because the operational hysteresis loops area is proportional to the load torque and on the other hand, the maximum flux density is also proportional to the input voltage. It means that in a constant input voltage, by variations of load, the operational hysteresis loops will change. However, the fourth assumption will not cause much error because of the small range of synchronous torque of the PMHS motors. In the following, the design procedure of the disc-type PMHS is presented. The input data of the design algorithm determined by the user is given in Table 1.

Table 1. Input data of the design algorithm.

Description	Quantity
Output power	P_{out}
Contribution ratio	n_p
Terminal voltage	V_t
Number of phases	m
Frequency	f
Rotor speed	n_m

Having the contribution ratio of the hysteresis motor n_p in the PMHS motor, the output power resulted from the hysteresis disc can be calculated as follows:

$$P_{out,Hys} = n_p P_{out}. \tag{1}$$

The mechanical torque resulted from the hysteresis disc T_{Hys} is formulated as:

$$T_{Hys} = \frac{P_{out,Hys}}{2\pi f \frac{2}{p}}. \tag{2}$$

For all hysteresis materials, the elliptic approximation of their hysteresis loops can be achieved by some experiments. The specifications of the elliptic approximation of hysteresis loops for the hysteresis material used

in this article are given in [10]. By choosing a value for the amplitude of magnetic flux density in hysteresis disc $B_{m,Hys}$, all the parameters of the operational hysteresis loop of the PMHS motor corresponding to this amplitude are obtained. These parameters include the magnetic permeability of the hysteresis disc μ, the hysteresis delay angle α, and the area of the hysteresis loop E_h. Based on the relation given in [19] between output torque of hysteresis motor T_{Hys}, the volume of the hysteresis disc V, and the area of the elliptic hysteresis loop E_h, V can be extracted here from T_{Hys} and E_h as follows:

$$V = \frac{4\pi T_{Hys}}{pE_h}. \tag{3}$$

Now, let D_o and D_i respectively represent the outer and inner diameters of hysteresis disc, or in other words, the outer and inner diameters of the stator core and PM disc. Their ratio (D_i / D_o) is also denoted as λ whose value is determined by empirical rules. By adopting an initial value for D_o, an initial value is calculated for D_i:

$$D_i = \lambda D_o. \tag{4}$$

Having the volume of the hysteresis disc from (3) as well as the value of λ and the initial value of D_o, an initial value is calculated for the thickness of the hysteresis disc t_r using the following equation:

$$t_r = \frac{4V}{\pi D_o^2(1-\lambda^2)}. \tag{5}$$

If the value obtained for t_r is reasonable magnetically and mechanically, the design procedure continues, otherwise, the value of D_o should be corrected. It is important to note that as the thickness of the hysteresis disc decreases, the amplitude of magnetic flux density inside it increases. This makes the motor hysteresis loop larger and consequently the motor torque, power factor and efficiency increase. On the other hand, there are many mechanical constraints in construction, heat treatment and assembly of a thin hysteresis disc. Therefore, a trade-off must be made for adopting the appropriate values of D_o and t_r.

Now, let us calculate the number of turns of the equivalent sinusoidal winding per phase N_s. For this purpose, it is necessary to consider its relation with the excitation voltage e_f induced by the hysteresis disc in the armature winding of phase 'a', as formulated in [10]:

$$e_f = -\frac{N_s L_e t_r B_{m,Hys} \pi \omega_e}{2a} cos(\omega_e t - \phi_0). \tag{6}$$

In which t, a, L_e and ω_e are time, number of parallel paths of each phase, radial length of the stator ($R_o - R_i$), and the electrical angular frequency, respectively. The phase angle ϕ_0, is also formulated as [10]:

$$\phi_0 = \frac{\pi}{2} + tan^{(-1)}\left(\frac{\frac{2R_{avg}}{p\mu} sin\alpha}{\frac{2R_{avg}}{p\mu} cos\alpha + \frac{gpt_r}{2\mu_0 R_{avg}}}\right), \tag{7}$$

where R_{avg}, g and μ_0 are the average radius of hysteresis disc, airgap length and magnetic permeability of air, respectively.

Let E_f be the peak amplitude of e_f in (6). Then, by adopting an initial value for E_f, an initial value is calculated for N_s using the following equation:

$$N_s = \frac{2aE_f}{L_e t_r B_{m,Hys} \pi \omega_e}. \tag{8}$$

The RMS value of armature current per phase is calculated as [10]:

$$I_s = \frac{B_{m,Hys}\sqrt{\left(\frac{gpt_r}{2\mu_0 R_{avg}}\right)^2 + \left(\frac{2R_{avg}}{p\mu}\right)^2 + \frac{2gt_r}{\mu_0\mu}cos\alpha}}{\frac{mN_s\sqrt{2}}{2pa}}. \tag{9}$$

By adopting a rational value for the current density J_s, the cross sectional area of conductors S_{cond} is:

$$S_{cond} = \frac{I_s}{J_s}. \tag{10}$$

Thus, by assuming a round conductor for stator windings, its diameter is calculated as:

$$d_{cond} = 2\sqrt{\frac{S_{cond}}{\pi}}. \tag{11}$$

By choosing a reasonable value for the thickness of conductor insulation d_{insu}, the wire diameter is obtained, and thus the number of winding layers N_{layer} and the winding thickness L_w are calculated:

$$d_{wire} = d_{cond} + d_{insu}, \tag{12}$$

$$N_{layer} = \frac{2N_s m d_{wire}}{\pi D_i}, \tag{13}$$

$$L_w = N_{layer} d_{wire}. \tag{14}$$

In this way, the initial values of all the parameters of armature windings as well as the dimensional specifications of hysteresis disc have been calculated. Now, let calculate the initial values of the dimensions of the stator core and PM disc. According to the flux continuity law, the airgap flux density at the hysteresis disc side $B_{g,Hys}$ is obtained as follows:

$$B_{g,Hys} = \frac{2B_{m,Hys}t_r}{\frac{2}{p}\pi R_{avg}}. \tag{15}$$

Again, by using the flux continuity law and adopting a rational value for the amplitude of magnetic flux density in stator core B_{cs}, the part of the stator core axial thickness through which the magnetic flux of hysteresis disc passes $L_{s,Hys}$ is calculated as follows:

$$L_{s,Hys} = \frac{\pi B_{g,Hys} D_o (1+\lambda)}{4pB_{cs}}. \tag{16}$$

The airgap flux density at the side of the PM disc can also be calculated from the following formula [20]:

$$B_{g,PM} = \frac{2\sqrt{2}pP_{out,PM}}{\pi K_w m f N_s I_s \eta D_o^2 (1-\lambda^2)} \tag{17}$$

In which η and K_w denote the efficiency of the PM disc and winding factor, respectively. Also, $P_{out,PM}$ represent the contribution of the PM disc to the output power that is calculated as follows:

$$P_{out,PM} = (1-n_p)P_{out}. \tag{18}$$

Now, the axial length of PMs l_{pm} is calculated as the root of the following equation [20]:

$$\sum_{n=1,3,\dots}^{\infty}(\frac{2B_r}{n\pi}sin(\frac{\alpha_i n\pi}{2})\frac{1-e^{\frac{-2n\pi l_{pm}}{\tau_p}}}{1-e^{\frac{-2n\pi(g+l_w+l_{pm})}{\tau_p}}}(e^{\frac{n\pi(-g-0.5l_w)}{\tau_p}}+e^{\frac{-n\pi(g+1.5l_w)}{\tau_p}}))-B_{g,PM}=0, \tag{19}$$

where B_r is the remanence of PMs, and τ_p and α_i stand for the pole pitch at the average radius and the ratio of PM width (at the average radius) to τ_p, respectively. We have:

$$\tau_p=\frac{\pi}{p}R_{avg}. \tag{20}$$

By using the flux continuity law for the third time, the part of the stator core axial thickness through which the magnetic flux of PM disc passes $L_{s,PM}$ is calculated as follows:

$$L_{s,PM}=\frac{\pi B_{g,PM}D_o(1+\lambda)}{4pB_{cs}}. \tag{21}$$

The total axial thickness of stator thus equals to:

$$L_s=L_{s,Hys}+L_{s,PM}. \tag{22}$$

To calculate the axial thickness of the magnet holder disc, we need the attainable flux density at the surface of magnet attached to the back-iron B_u, which can be calculated as follows [20]:

$$B_u=\frac{2}{\alpha_i\tau_p}\sum_{n=1,3,\dots}^{\infty}(\frac{4B_r\tau_p}{(n\pi)^2}sin^2(\frac{\alpha_i n\pi}{2})(1-\frac{(1-e^{\frac{-2n\pi(g+l_w)}{\tau_p}})e^{\frac{-n\pi l_{pm}}{\tau_p}}}{1-e^{\frac{-2n\pi(g+l_w+l_{pm})}{\tau_p}}})). \tag{23}$$

Thereby, based on the flux continuity law and by adopting a reasonable value for the flux density amplitude inside the magnet holder disc B_{cr}, the axial thickness of the magnet holder disc L_r is calculated as follows:

$$L_r=\frac{\pi\alpha_i B_u D_o(1+\lambda)}{8pB_{cr}}. \tag{24}$$

Now the initial design process of the disc-type PMHS motor finishes. It should be remembered that all the design parameters have been calculated above based on an initially adopted value of E_f. Having the values of these parameters, the parameters of the equivalent circuit of the motor (according to that presented in [10]) are obtained. Then by establishing the equivalent circuit of the motor, it is verified whether the adopted value of E_f yields the previously known terminal or not (This is measured by the condition of convergence error as $\varepsilon_v=0.0001$). If yes, the design process ends, otherwise, the value of E_f is modified and the procedure repeats until this criterion is met. For better understanding, the flowchart of the design algorithm is displayed in Figure 2.

Regarding the convergence of the algorithm, for the 20% combination ratio n_p, convergence occurred after 1150 iterations (for the other n_p values it was about the same). It should be noted that this number of iterations also depends on the value of step of E_f (In the proposed algorithm, the bisection method is used, in which, after each change of the error sign, the value of step of E_f is halved). Each convergence of this algorithm

takes about 3.5 hours (for a personal PC). This value will vary depending on the processor system. Most of this time is spent calculating the machine leakage reactance. Due to the new structure of the machine and also to achieve more accuracy, finite element software has been used to calculate the leakage reactance. Thus, in each iteration, it is necessary to call the finite element software. Because the structure of the machine under study is known as one of the new structures, accurate and reliable analytical relationships for its leakage reactance are not provided. It can be said that the rest of the algorithm steps takes less than a few minutes.

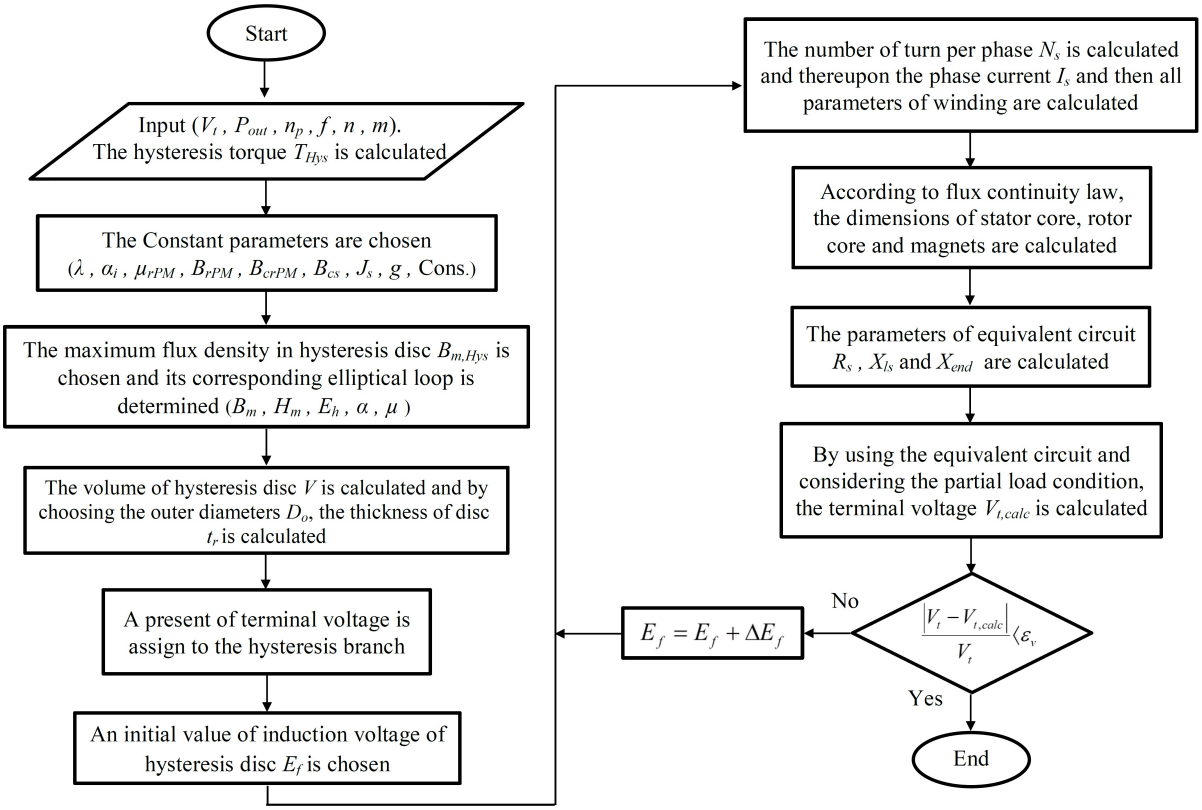

Figure 2. Flowchart of the design algorithm of disc-type PMHS motor.

It should be noted that the proposed algorithm properly decreases the dimensional limitations in the PMHS motor. In fact, this algorithm designs a HS motor and then designs a PM motor with dimensional constrains created by the HS motor. Therefore, the dimensional conflict that exists in hybrid motors will disappear.

3. Results of implementing the proposed design algorithm

In this section, the results of implementing the proposed algorithm in MATLAB for designing of a prototype disc-type PMHS motor are presented. The input data of the design program are presented in Table 2. In this design procedure, the contribution ratio is chosen 20 percent. The smaller the contribution ratio of hysteresis torque in the output power, the smaller the size of the hysteresis disc and the lower the cost and manufacturing constraints. On the other hand, if the hysteresis torque is too low, it will not be able to withstand the annoying torques caused by the magnets and therefore cannot drive the motor to synchronous speed. Similarly, the higher the contribution ratio of hysteresis torque in the output power, the more easily and in the shortest time the

motor will reach synchronous speed and hysteresis disc can also easily play the role of damper at synchronous speed. However, increasing the hysteresis torque will also increase its dimensions. More specifically, as the contribution ratio of hysteresis torque in the output power increases, we will need a hysteresis disc with a very large diameter and thin thickness. The hysteresis disc, after the turnery operation, needs to be heated and hardened so that its magnetic fields are formed and have the features of hysteresis. If the diameter of the disc is very large and its thickness is thin, it will warp or crack during heat treatment. In addition, increasing the contribution ratio of hysteresis torque means decreasing the contribution ratio of the magnet torque. This means that the thickness of the magnets must also be very small, which is very expensive. Therefore, it is necessary to make a compromise in the process of manufacturing this motor, which will have different results depending on the application and the desired cost. With this explanation, in this paper, according to our practical experiences as well as our existing equipment for manufacturing hysteresis discs and magnets, 20% has been selected for the contribution ratio of hysteresis torque in the output power. It should be noted that this value can be selected continuously in the range of 0 to 100. These explanations were added to text of manuscript. The hysteresis disc is made of an appropriate hysteresis material with the commercial brand VCN-150, which is composed of Fe-Cr-Ni-Mo-C alloy.

Table 2. Input data of the proposed design algorithm.

Description	Quantity
Motor output power	$P_{out} = 200\ W$
Contribution ratio	$n_p = 20\ \%$
Terminal voltage	$V_{t,L-L} = 130\ V$
Number of phases	$m = 3$
Frequency	$f = 50\ Hz$
Rotor speed	$n_m = 1500\ rpm$

After applying the input data of Table 2 to the proposed design algorithm, the resulted design parameters are listed in Table 3. Now, the variations of the principal design parameters are analyzed while the contribution ratio of hysteresis disc n_p changes. For this purpose, the prototype motor is designed based on the design requirements of Table 2 while the value of n_p varies from 0.1 to 0.8 and the results are presented.

It should be noted that some parameters of the motor such as airgap length, the type of winding, its connection, etc. are maintained constant while changing n_p. Figure 3 shows the variations in the dimensions of the motor for the changes in n_p. It can be observed that as n_p increases, the dimensions of the PM rotor and the total axial length of the motor decrease and the dimensions of the hysteresis disc and the external diameter of the motor enlarge.

The resulted changes in the performance parameters of the motor while changing n_p are illustrated in Figures 4 and 5. As shown in these figures, as n_p increases, the motor input current increases. The reason for this is that as the average radius of the hysteresis disc increases, its equivalent impedance decreases. This is also proved by (9). It is also apparent that when n_p increases, the behavior of the PMHS motor becomes more similar to the hysteresis motor and its power factor and efficiency decrease.

According to the results presented in this section, it can be concluded that depending on the application of the PMHS motor, there should be a compromise in determining the contribution ratio. This can be achieved by defining a suitable objective function and implementing an optimization process.

Table 3. Principal results of the design algorithm of the disc-type PMHS motor.

Description	Quantity
Number of winding turns per phase	$N_s = 368$
Number of winding layers per phase	$N_{layer} = 4$
Number of turn per winding layer	$N_c = 92$
Number of coils per phase	$N_{coil} = 2$
Connection type of armature windings	*Star*
Type of armature winding	*Lapwinding*
Coil pitch	*Complete*
Wire diameter	$d_{wire} = 0.7\ mm$
Inner diameter of hysteresis disc	$D_i = 150\ mm$
Outer diameter of hysteresis disc	$D_o = 250\ mm$
Thickness of hysteresis disc	$t_r = 4\ mm$
Axial thickness of stator core	$L_s = 20\ mm$
Remanence of PMs	$B_{r,PM} = 0.4\ T$
Axial length of PMs	$l_{pm} = 5\ mm$
Axial thickness of magnet holder disc	$L_r = 10\ mm$
Airgap length	$g = 1.2\ mm$

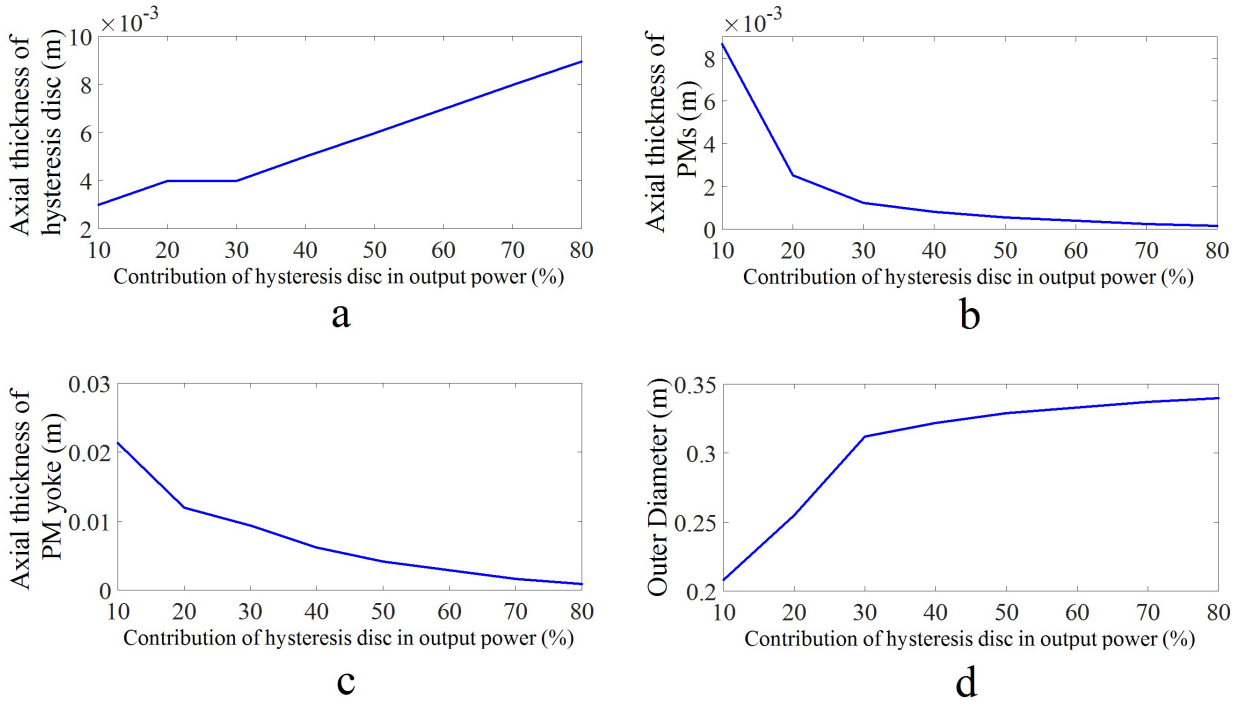

Figure 3. Variations of the motor dimensions while changing n_p, a) axial length of hysteresis disc, b) axial length of PMs, c) axial length of magnet holder disc, d) outer diameter of the motor.

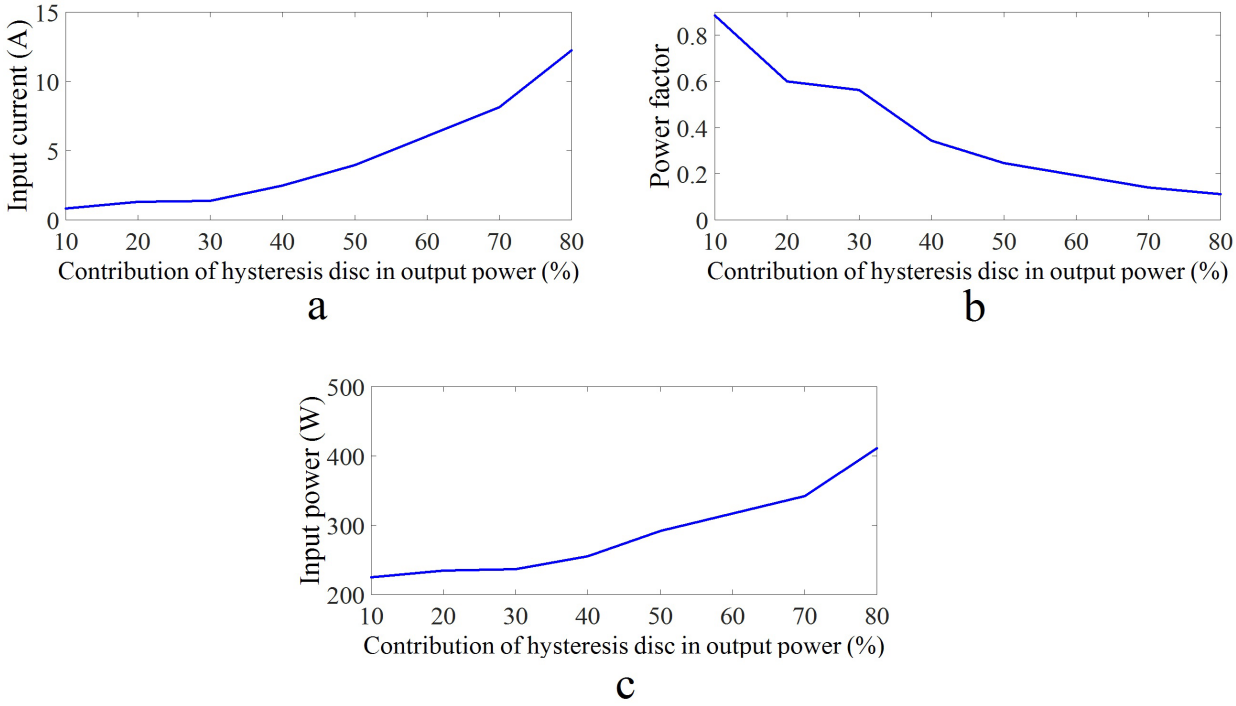

Figure 4. Variations of the performance parameters of the motor while changing n_p, a) input current of the motor, b) power factor, c) input power.

4. Results of simulation and experiments

In this section, the results of simulation and experiments are presented for a prototype disc-type PMHS motor that is fabricated based on the input data of Table 3. Figure 6 shows the various components and the final assembly of the manufactured PMHS motor. As indicated in this figure, the magnet holder disc is a ferromagnetic material to transmit the flux of the magnets with minimal weakening. The hysteresis disc holder is made of a nonmagnetic material, causing the flux to peripherally close its path in the hysteresis disc. The stator core is also made using a rolled ferromagnetic sheet. It should be noted that both discs (hysteresis discs and PM discs) are connected to each other through a common shaft rotating at an equal speed. As a result, the hysteresis disc provides the starting torque for the PM disc.

In the following, the most important performance characteristics of the prototype motor, which are derived from the analytical model and real tests in maximum synchronous torque conditions, are presented. These characteristics are plotted for input voltages between 110 and 200 V. It is necessary to mention that the proposed PMHS motor is line-start and in our test stages, it was directly supplied. To provide different voltage levels, a tap-changer transformer has been used. In this method, after adjusting the transformer at a voltage of the desired amplitude (frequency is constant and will be equal to 50 Hz), this voltage is applied directly to the motor. After the motor reaches the synchronous speed, the motor is loaded by the DC generator (to achieve the maximum load, in addition to the DC generator, frictional load is required). After reaching the maximum load conditions, the values from the measuring devices are recorded. Due to the small torque range of the hysteresis motors it needs high-tech measurement and loading tools to provide the maximum torque conditions but in this work it has been attempted to achieve maximum torque conditions by applying more friction to the shaft.

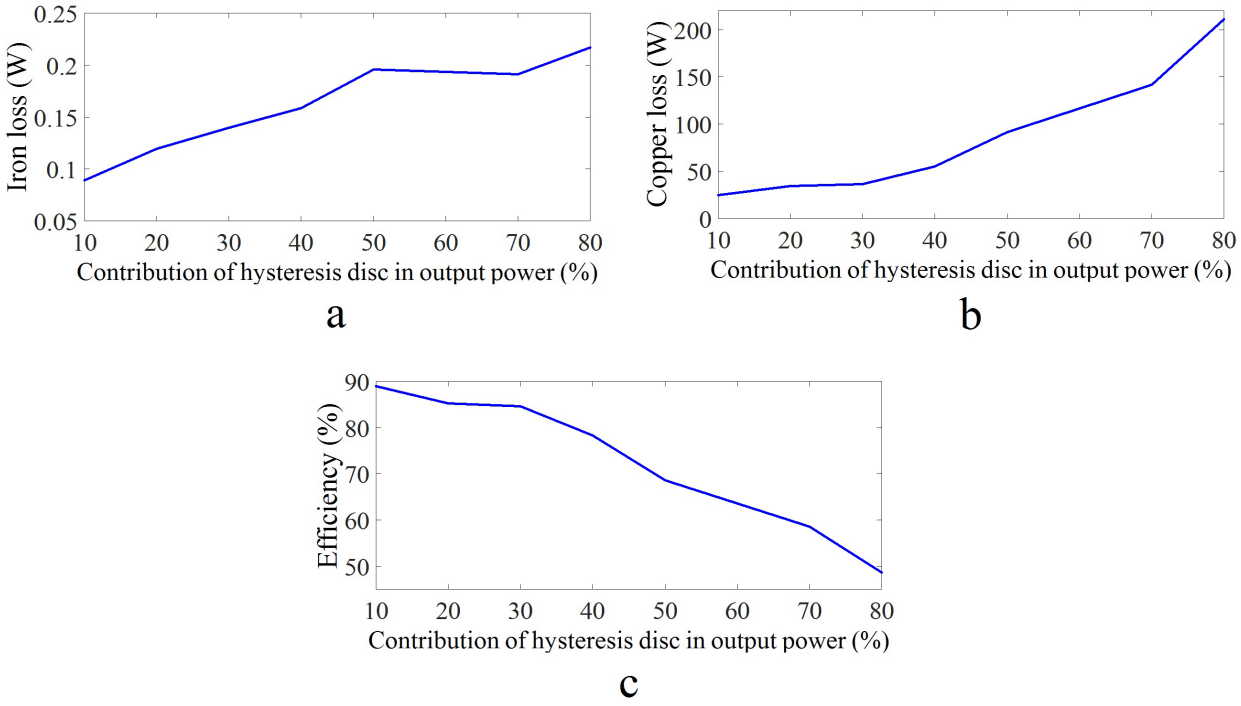

Figure 5. Variations of the performance parameters of the motor while changing n_p , a) iron losses, b) copper losses, c) efficiency.

The variations of the peak amplitude of the motor input current with respect to the terminal line voltage obtained from the analytical model and experiment are illustrated in Figure 7. As can be seen from this figure, increasing the input voltage will increase the input current. This is easily understood by referring to the equivalent circuit of the machine (presented in [10]). The relation between the input power factor and the terminal voltage is also shown in Figure 8. It should be noted that increasing the input voltage causes the operational hysteresis loop of motor to become larger. This means that the behavior of the hybrid machine tends towards the hysteresis motor, which leads to a reduction in the power factor. In the other word, as the input voltage increases (and, consequently, increasing the maximum flux density), the value of equivalent impedance of the hysteresis disc increases and its lag effect dominates the entire motor. Figure 9 displays the three-phase input power variation curves versus the terminal voltage. The variations of the copper losses and efficiency of the motor versus its terminal voltage are also depicted in Figure 10 and Figure 11, respectively. Noticeable increase occurred in efficiency is counted as benefit of proposed method.

The reason for the difference between theoretical and experimental results can be stated as follows:

1) The stator MMF waveform is considered sinusoidally in theoretical relations. Applying this approximation will lead to significant simplicity in relationships and solving equations. It should be noted that due to the increase in effective airgap in slotless structures, this approximation will not produce much error.

2) In theoretical calculations, the hysteresis loop of the rotor material is approximated by an ellipse. This is done to avoid the complexity of the calculations and reduce the execution time of the algorithm. Accurate models for the hysteresis loop approximation, such as the Preisach model, in addition to complicating the calculations, sometimes lead to algorithm divergence.

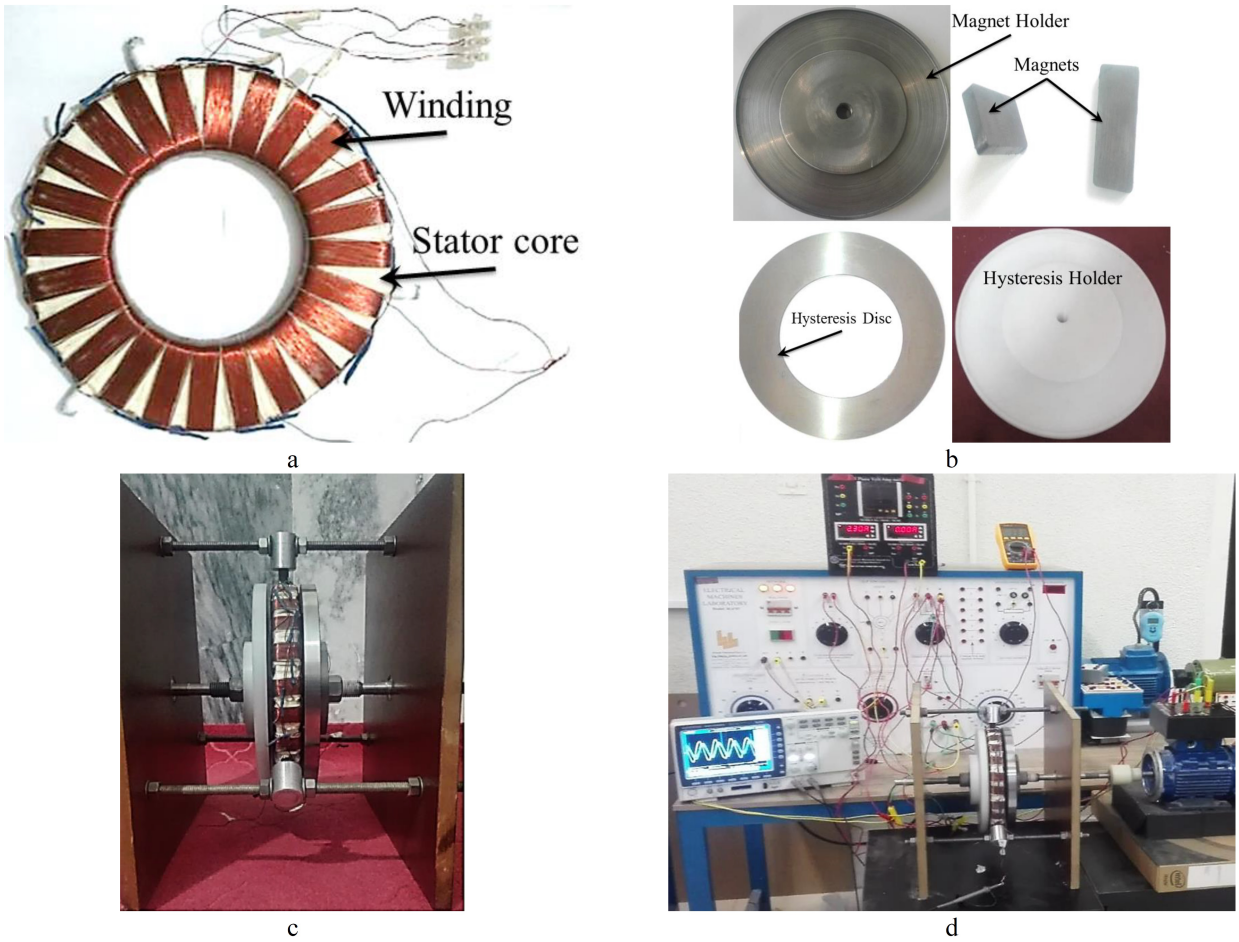

Figure 6. Various components and final assembly of the fabricated PMHS motor, a) disc-type stator core with thyroidal winding, b) rotor set, c) the final assembly of disc-type PMHS motor, d) test stand.

3) Providing maximum synchronous torque conditions in practical tests is difficult and therefore causes errors in the results.These errors are greatly reduced by repeating several times the test.

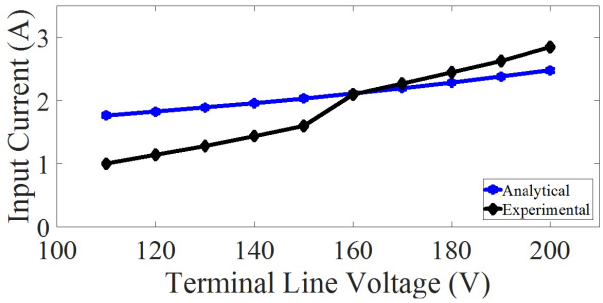

Figure 7. Variations of input current versus terminal voltage.

The characteristics obtained from the analytical model and experiments show that as the input voltage increases, due to the increase in the size of the operational hysteresis loop of the motor, its input current, input

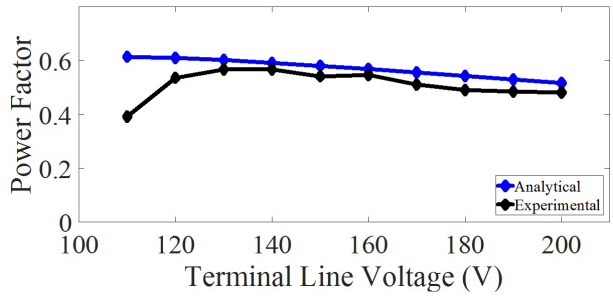

Figure 8. Variations of power factor versus terminal voltage.

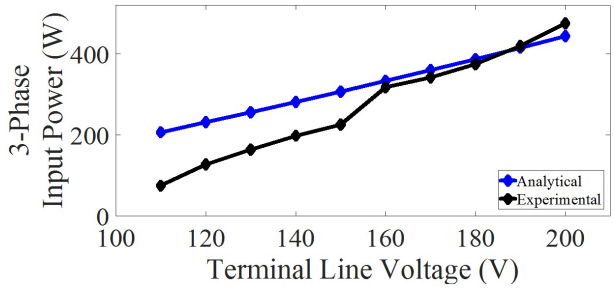

Figure 9. Variations of input power versus terminal voltage.

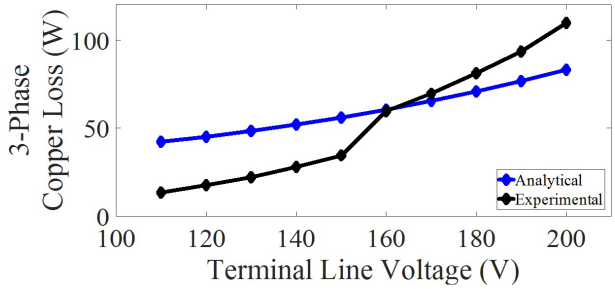

Figure 10. Variations of copper loss versus terminal voltage.

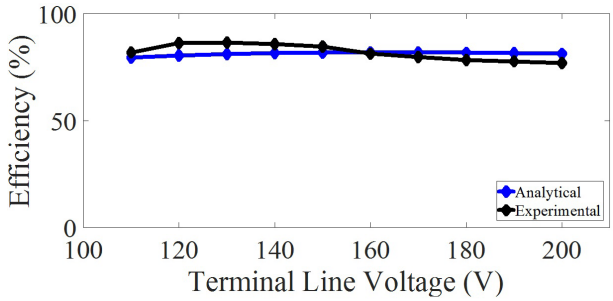

Figure 11. Variations of motor efficiency versus terminal voltage.

power and losses all increase. This consequence is valid for all types of hysteresis and PMHS motors.

Comparing the analytical and experimental results with those obtained from the design algorithm (in the

previous section) for the terminal voltage of 130 V and the contribution ratio (n_p) of 0.2 obviously demonstrates the validity of the proposed design algorithm.

5. Conclusion

Combining the hysteresis motor with permanent magnet motor can lead to a motor with unique features that can overcome the limitations of the industries that are dependent on hysteresis motor. This goal is achievable by the correct and flexible design and choosing an appropriate structure for the hybrid motor. So far, no design algorithm for this hybrid motor has been presented in any reference. In this paper, a new design algorithm for the disc-type PM-hysteresis hybrid motor was introduced. It has also been demonstrated that by using this design algorithm and adopting the disc-type structure for the PMHS motor, the advantages of both hysteresis and PM motors in the resulted hybrid motor can be retained. In addition, the proposed algorithm of this paper provides the user the ability to determine the contribution ratio of each motor to the output power of the hybrid motor. Therefore, the user can easily determine, based on the required application, the dominant influence of each of two motors in the PMHS motor. The results of experiments and simulations strongly confirmed the validity of the proposed design algorithm.

References

[1] Jagiela M, Garbiec T, Kowol M. Design of high-speed hybrid hysreresis motor rotor using finite element model and decision process. IEEE Transaction on Magnetics 2014; 50 (2): 861-864. doi: 10.1109/TMAG.2013.2284018

[2] Wakui G. Hysteresis motor with reaction torque and its analysis. Electrical Engineering in Japan 1978; 98 (5): 58-67. doi: 10.1002/eej.4390980508

[3] Rahman M, Osheiba A, Little T. Effects of samarium cobalt permanent magnet on the performance of polyphase hysteresis-reluctance motors. IEEE Transaction on Magnetics 1984; MAG-20 (5): 1765-1767. doi: 10.1109/TMAG.1984.1063477

[4] Rahman M, Osheiba A. Steady-state performance analysis of polyphase hysteresis-reluctance motors. IEEE Transactions on Industry Applications 1985; IA-21 (4): 659-663. doi: 10.1109/TIA.1985.349723

[5] Rahman M, Osheiba A. Improved performance of polyphase hysteresis-reluctance motors fed from single-phase supplies. IEEE Transactions on Industry Application 1990; 26 (1): 130-136. doi: 10.1109/28.52684

[6] Rahman M. Combination hysteresis reluctance permanent magnet motor. United States of America Patent, 16 February 1993. Patent Number: 5,187,401.

[7] Rahman M, Qin R. Starting and synchronization of permanent magnet hysteresis motors. IEEE Transactions on Industry Application 1996; 32 (5): 1183-1189. doi: 10.1109/28.536881

[8] Qin R, Rahman M. Magnetic equivalent circuit of PM hysteresis synchronous motor. IEEE Transactions on Magnetics 2003; 39 (5): 2998-3000. doi: 10.1109/TMAG.2003.816719

[9] Kurihara K, Rahman M. Transient performance analysis for permanent-magnet hysteresis synchronous motor. IEEE Transactions on Industry Applications 2004; 40 (1): 135-142. doi: 10.1109/TIA.2003.821794

[10] Behniafar A, Darabi A. Analytical modeling of disc type permanent magnet hysteresis motor in steady state operational conditions. COMPEL: The International Journal for Computation and Mathematics in Electrical and Electronic Engineering 2017; 36 (4): 991-1007. doi: 10.1108/COMPEL-07-2016-0315

[11] Behniafar A, Darabi A. A new semianalytical method for analysis of the disc-type permanent magnet hysteresis motor in steady-state operational conditions. Turkish Journal of Electrical Engineering & Computer Sciences 2018; 26 (1): 542-553. doi: 10.3906/elk-1702-264

[12] Rahman M, Qin R. A permanent magnet hysteresis hybrid synchronous motor for electric vehicles. IEEE Transactions on Industrial Electronics 1997; 44 (1): 46-53. doi: 10.1109/41.557498

[13] Qin R, Rahman M. DSP based torque and speed controls of the permanent magnet hysteresis synchronous motor. In: IEEE International Electric Machines and Drives Conference Record; Milwaukee, WI, USA; 1997. doi: 10.1109/IEMDC.1997.604181

[14] Qian J, Rahman M. Analysis of field oriented control for permanent magnet hysteresis synchronous motors. IEEE Transactions on Industry Applications 1993; 29 (6): 1156-1163. doi: 10.1109/28.259727

[15] Nasiri-Gheidari Z, Lesani H, Tootoonchian F. A new hunting control method for permanent magnet hysteresis motors. Iranian Journal of Electrical & Electronic Engineering IJEEE 2006; 2 (3): 121-130.

[16] Lesani H, Darabi A, Nasiri Gheidari Z, Tootoonchian F. Very fast field oriented control for permanent magnet hysteresis synchronous motor. Iranian Journal of Electrical & Electronic Engineering 2006; 2 (1): 34-40.

[17] Rabbi S, Rahman M. Equivalent circuit modeling of a hysteresis interior permanent magnet motor for electric submersible pump. IEEE Transactions on Magnetics 2016; 52 (7): 1-4. doi: 10.1109/TMAG.2016.2525007

[18] Rabbi F, Halloran M, LeDrew T, Matchem A, Rahman M. Modeling and V/F control of a hysteresis interior permanent magnet motor. IEEE Transactions on Industry Applications 2016; 52 (2): 1891-1901. doi: 10.1109/TIA.2015.2505666

[19] Darabi A, Sadeghi M, Hassannia A. Design optimization of multistack coreless disk-type hysteresis motor. IEEE Transactions on Energy Conversion 2011; 26 (4): 1081-1087. doi: 10.1109/TEC.2011.2162107

[20] Darabi A, Baghayipour M, Mirzahosseini R. An extended analytical algorithm for optimal designing of a TORUS-type non-slotted axial-flux permanent magnet motor. Journal of Control, Automation and Electrical Systems 2017; 28 (6): 748-761. doi: 10.1007/s40313-017-0337-8